SUPPLEMENTARY INFORMATION

Engineering the structural topology of pyrene-based conjugated polymers for the selective sorting of semiconducting single-walled carbon nanotubes

Kyoungtae Hwang, Dae-Hee Lim, Min-Hye Lee, Yeon-Ju Kim, Yeong-a Kim, Dongsung Yang, Younghyo Kim and Dong-Yu Kim*

K. Hwang, D. Yang, Y. Kim Prof. D. -Y. Kim*

School of Materials Science and Engineering (SMSE),

Research Institute for Solar and Sustainable Energies (RISE),

Gwangju Institute of Science and Technology (GIST)

123 Cheomdan-gwagiro Buk-gu, Gwangju 61005, Republic of Korea

E-mail: kimdy@gist.ac.kr

Dr. D.-H. Lim

Energy Materials Research Center

Korea Research Institute of Chemical Technology (KRICT)

141 Gajeong-ro, Yuseong-gu, Daejeon 34114, Republic of Korea

Dr. M.-H. Lee

Agency for Defense Development

Yuseong P.O.Box 35, Daejeon 34188, Korea

Y.-J. Kim,
Nanoscience and Technology Division, Argonne National Laboratory,
Lemont, Illinois 60439, United States.
Dr. Y.-A. Kim
LG Chem Ltd Basic Materials and Chemicals Research and Development Center, Yeosu,
Jeollanam-do, 59611, Repubilic of Korea.

CONTENTS

NMR spectra of compounds (1)–(5); high-temperature gel permeation chromatography analysis, thermal gravimetric and differential scanning calorimetry, cyclic voltammetry, 2D-grazing-incidence wide-angle X-ray diffractometry analysis of the prepared polymers; schematic of SWNT enrichment process; UV-vis-NIR spectra of polymer/single-walled carbon nanotube (SWNT) hybrids in toluene; G-band Raman spectra of polymer/SWNT hybrids in toluene; current output curves of carbon nanotube field-effect transistors (FET) with channel lengths of 5 and 10 μm prepared using the enriched SWNTs; atomic force microscopy images and height profiles of the FET device.

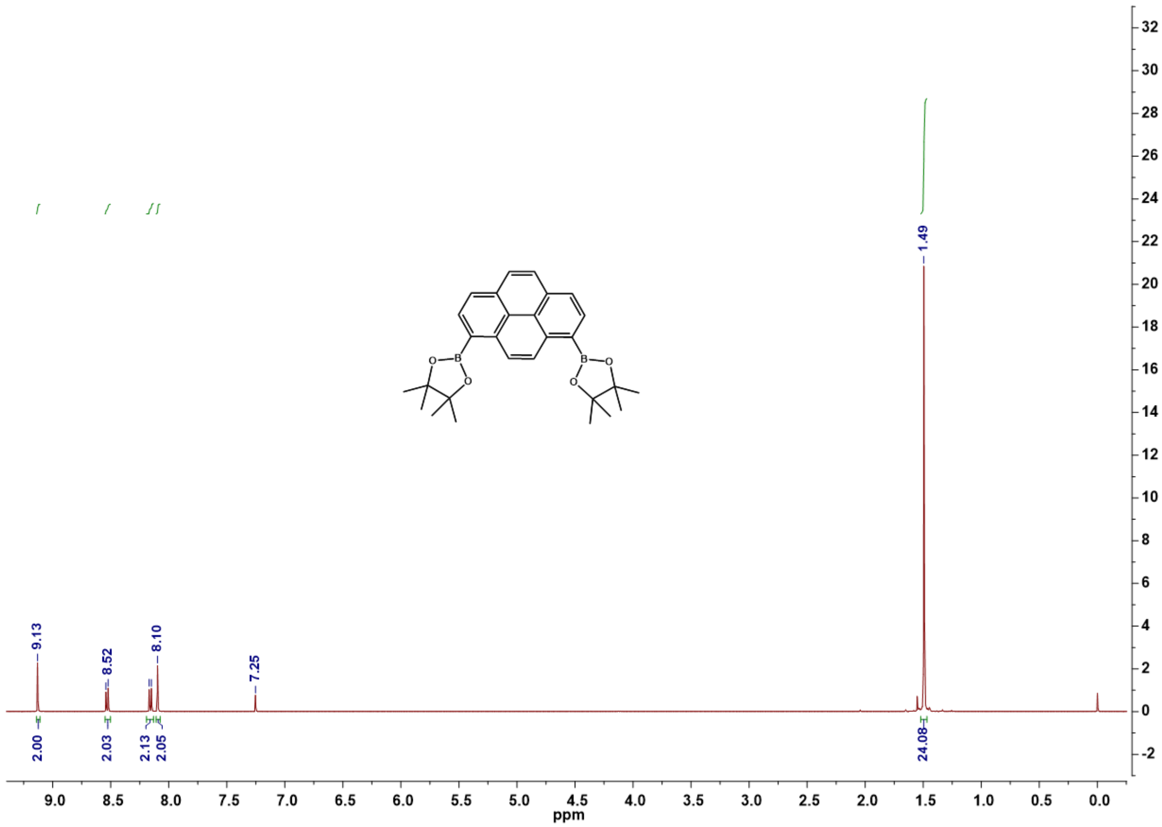

Figure S1. ^{1}H-NMR spectrum of 1,8-bis(4,4,5,5-tetramethyl-1,3,2-dioxaborolan-2-yl)pyrene (1) (400 MHz, $CDCl_3$): 9.13 (s, 2H), 8.52 (d, J=7.7 Hz 2H), 8.17 (d, J=7.6 Hz 2H), 8.10 (s, 2H), 1.49 (s, 24H).

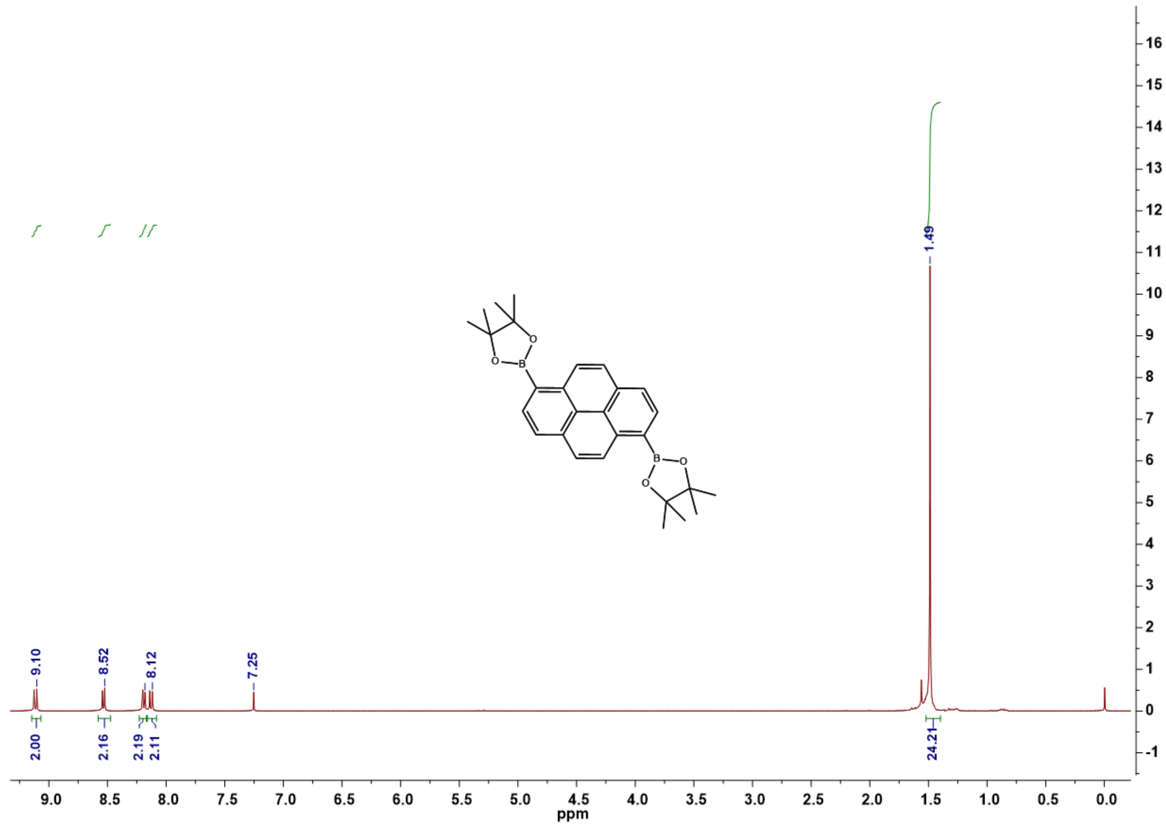

Figure S2. ^{1}H-NMR spectrum of 1,6-bis(4,4,5,5-tetramethyl-1,3,2-dioxaborolan-2-yl)pyrene (2) (400 MHz, $CDCl_3$): 9.10 (d, J=9.2 Hz, 2H), 8.52 (d, J=7.7Hz 2H), 8.17 (d, J=7.7Hz, 2H), 8.12 (d, J=9.2 Hz, 2H), 1.49 (s, 24H).

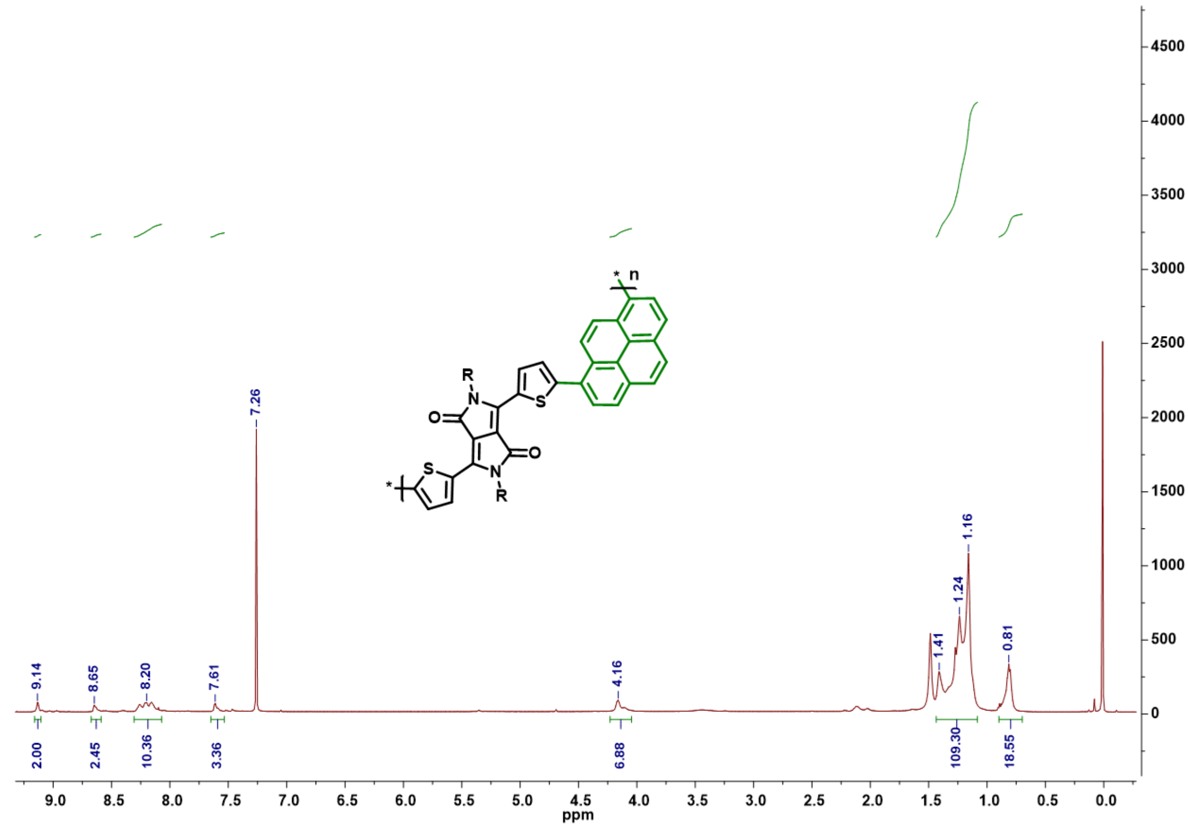

Figure S3. ^{1}H-NMR spectrum of P(1,8-pyDPP) (3) (400 MHz, $CDCl_3$): 9.14 (s, 2H), 8.65 (s, 2H), 8.20 (m, 10H), 7.61 (s, 3H), 4.16 (s, 4H), 1.24 (br, 109H), 0.81 (s, 18H).

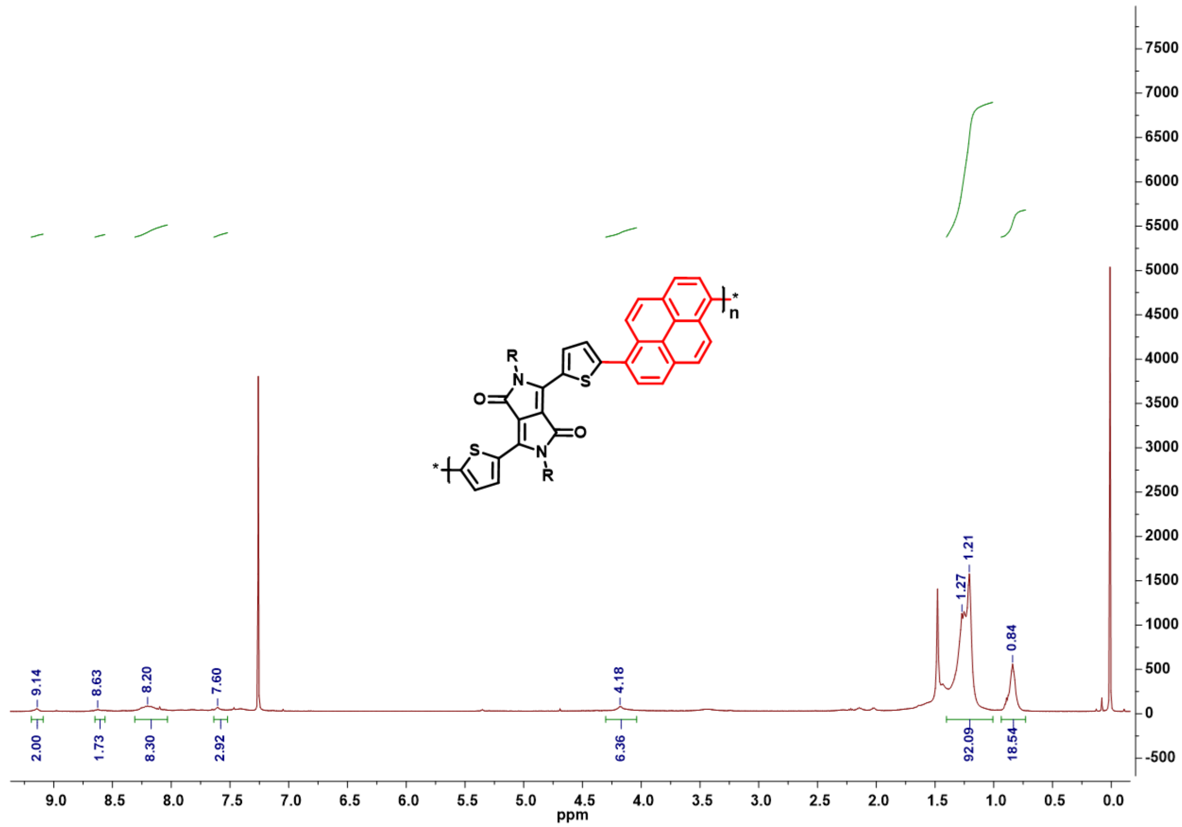

Figure S4. [1]H-NMR spectrum of P(1,6-pyDPP) (3) (400 MHz, $CDCl_3$): 9.14 (s, 2H), 8.63 (s, 2H), 8.30 (br, 8H), 7.61 (s, 3H), 6.36 (s, 4H), 1.21 (br, 92H), 0.84 (s, 18H).

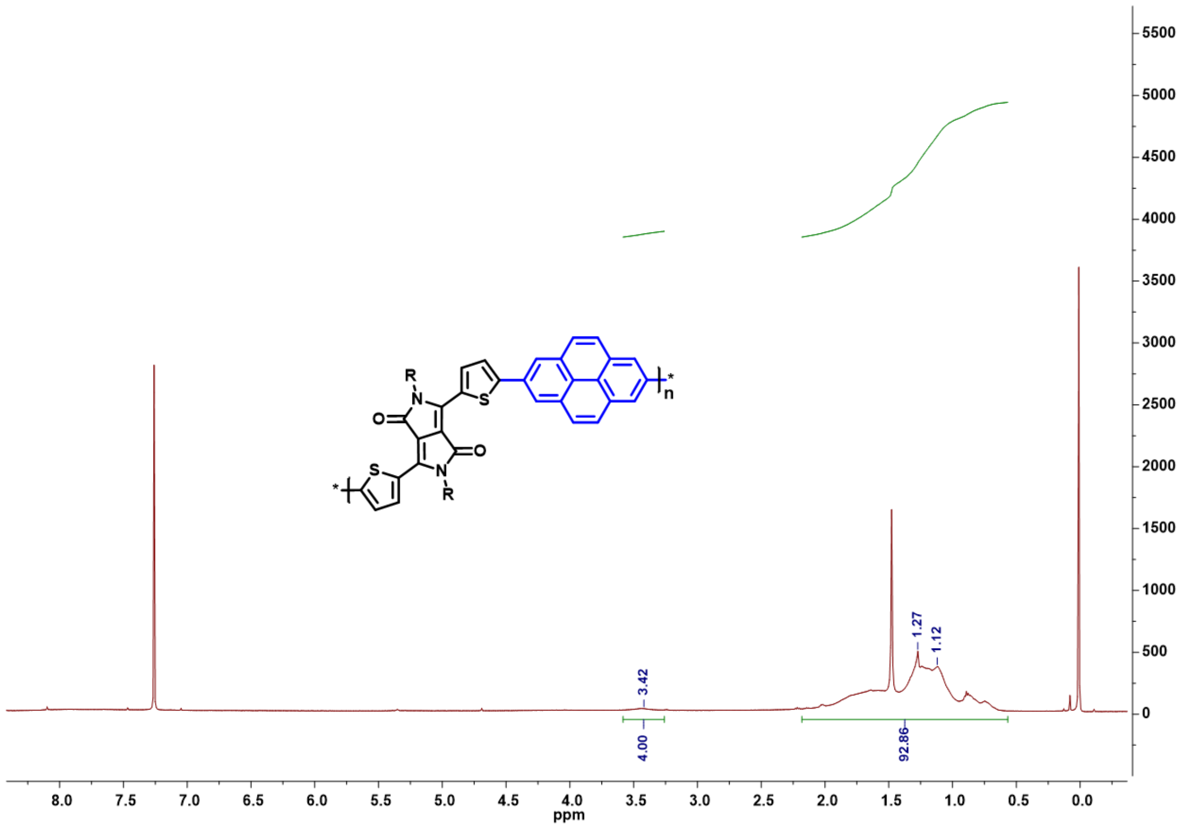

Figure S5. ^{1}H-NMR spectrum of P(2,7-pyDPP) (5) (400 MHz, $CDCl_3$): 3.42 (br, 4H), 1.12 (br, 92H).

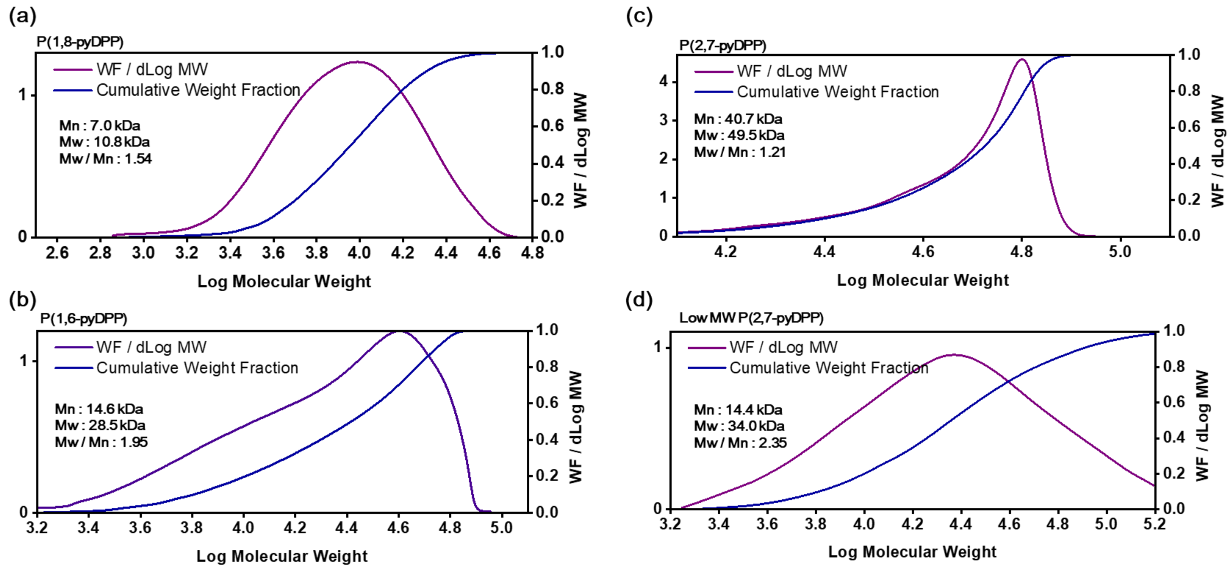

Figure S6. High-temperature gel permeation chromatography (HT-GPC) analysis of diketopyrrolopyrrole (DPP)-based conjugated polymers for (a) P(1,8-pyDPP), (b) P(1,6-pyDPP), (c) P(2,7-pyDPP) and (d) low molecular weight P(2,7-pyDPP).

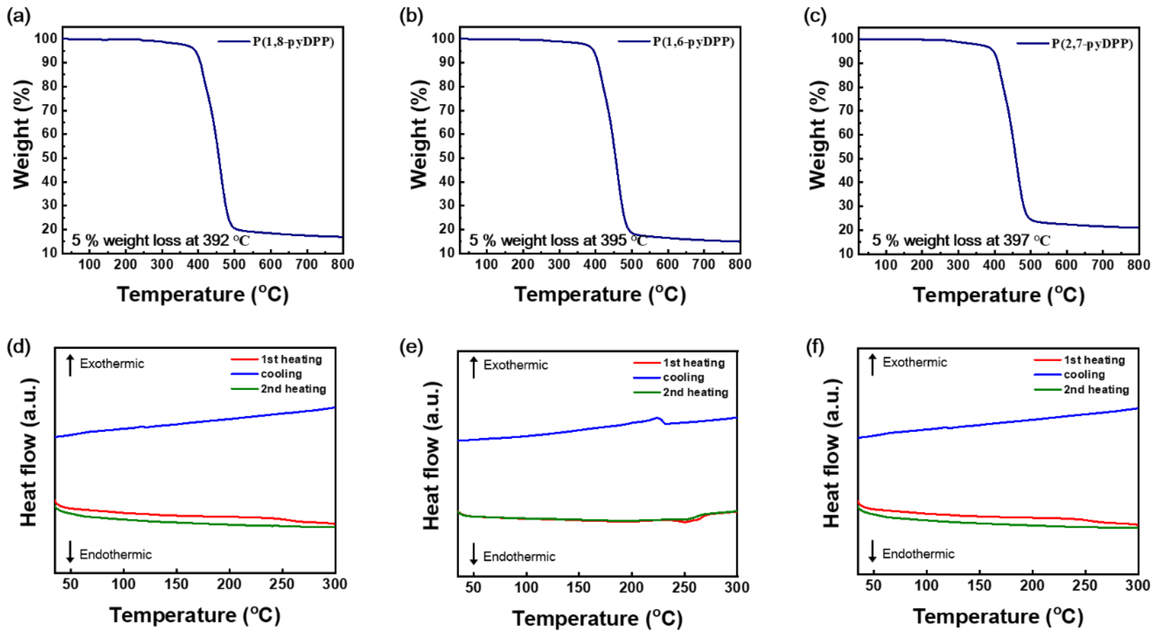

Figure S7. Thermal behavior of (a),(d) P(1,8-pyDPP), (b),(e) P(1,6-pyDPP), and (c),(f) P(2,7-pyDPP) obtained via thermogravimetric analysis (TGA) and differential scanning calorimetry (DSC) measurements.

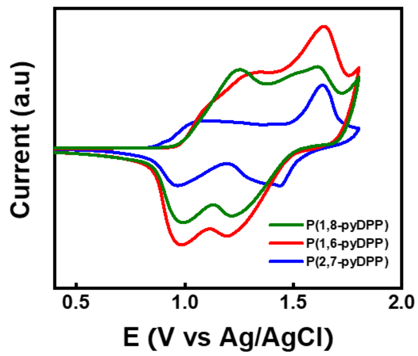

Figure S8. Cyclic voltammetry (CV) curves of P(1,8-pyDPP), P(1,6-pyDPP), and P(2,7-pyDPP) in 0.1 M n-Bu_4NPF_6 in anhydrous acetonitrile (scan rate: 50 mVs^{-1}).

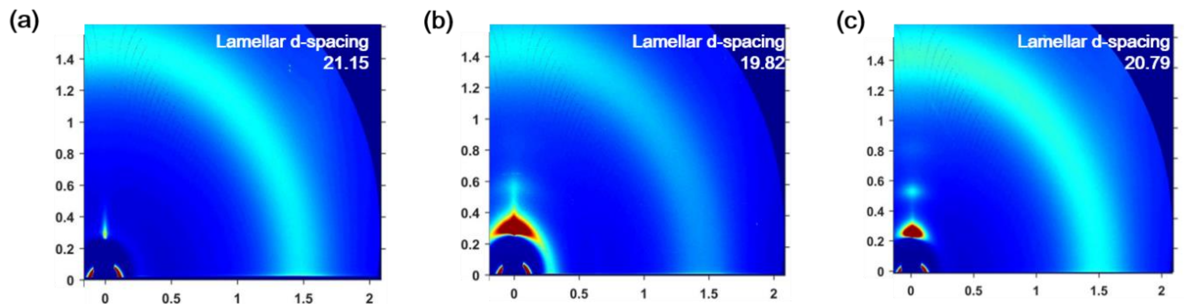

Figure S9. Grazing-incidence wide-angle X-ray diffraction (2D-GIWAXD) and out-of-plane 1D profiles of films of (a) P(1,8-pyDPP), (b) P(1,6-pyDPP), and (c) P(2,7-pyDPP).

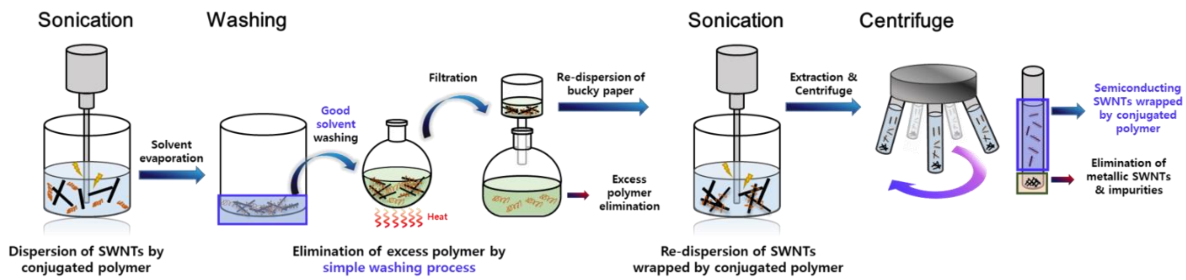

Figure S10. Enrichment process for the selective dispersion of semiconducting (sc)-SWNTs with minimal DPP-based polymer.

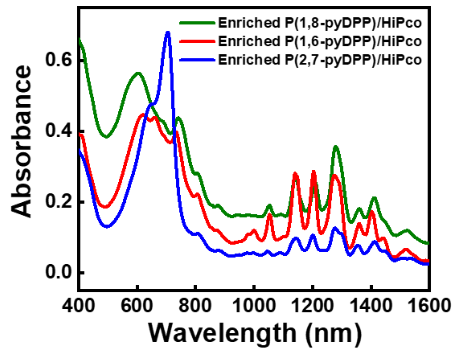

Figure S11. UV-vis-NIR absorbance spectra of the high-pressure carbon monoxide (HiPco) process SWNTs enriched by P(1,8-pyDPP), P(1,6-pyDPP), and P(2,7-pyDPP) in toluene.

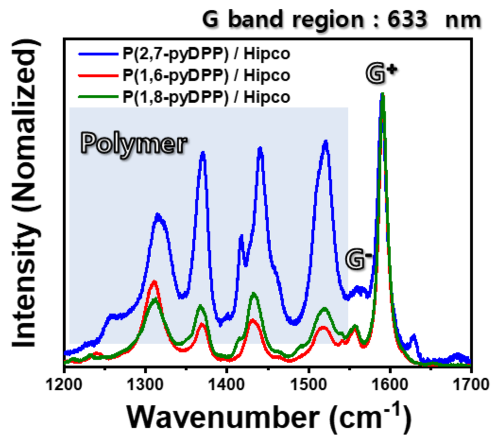

Figure S12. G-band region of Raman spectra obtained using a 633-nm laser for films of HiPco SWNT suspensions dispersed by P(1,8-pyDPP), P(1,6-pyDPP), and P(2,7-pyDPP) in toluene.

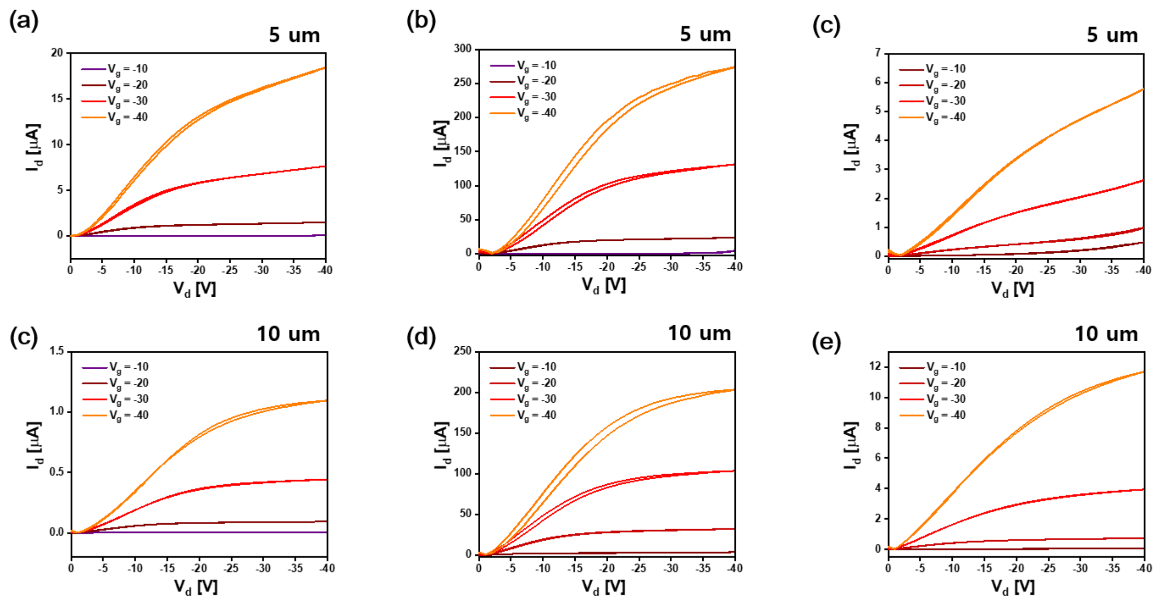

Figure S13. Output curves of carbon nanotube (CNT)-field effect transistors (FETs) with channel lengths of 5 and 10 μm for (a, c) P(1,8-pyDPP)/Hipco, (b, d) P(1,6-pyDPP)/Hipco, and (c, e) P(2,7-pyDPP)/Hipco hybrid films.

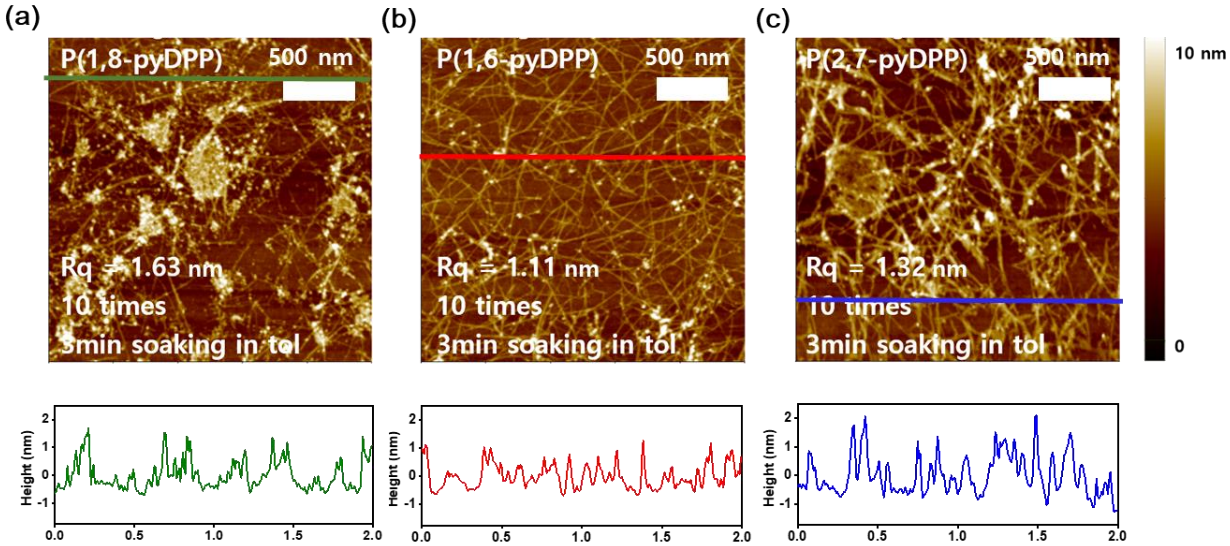

Figure S14. Atomic force microscopy (AFM) height images and surface profiles with a scan size of 2 μm × 2 μm in bottom-gate bottom-contact (BG/BC) FET devices fabricated using (a) P(1,8-pyDPP)/Hipco, (b) P(1,6-pyDPP)/Hipco, and (c) P(2,7-pyDPP)/Hipco hybrids.

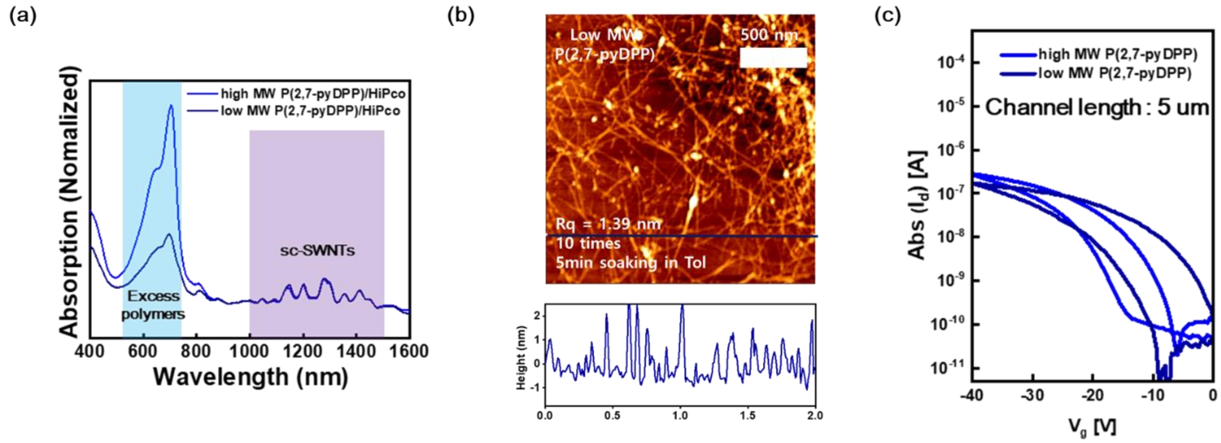

Figure S15. (a) UV-Vis-Nir absorption spectra of the sorted sc-SWNT solutions prepared by high molecular weight (MW) P(2,7-pyDPP) and low molecular weight (MW) P(2,7-pyDPP), (b) AFM images and (c) transfer curves in BG/BC FET devices fabricated by high MW P(2,7-pyDPP) and low MW P(2,7-pyDPP) / Hipco hybrids.